Impact on flight trajectory characteristics when avoiding the formation of persistent contrails for transatlantic flights

Yin, Feijia; Grewe, Volker; Frömming, Christine; Yamashita, Hiroshi

DOI
10.1016/j.trd.2018.09.017

Publication date
2018

Document Version
Final published version

Published in
Transportation Research Part D: Transport and Environment

Citation (APA)
Yin, F., Grewe, V., Frömming, C., & Yamashita, H. (2018). Impact on flight trajectory characteristics when avoiding the formation of persistent contrails for transatlantic flights. *Transportation Research Part D: Transport and Environment*, *65*, 466-484. https://doi.org/10.1016/j.trd.2018.09.017

Transportation Research Part D 65 (2018) 466–484

Contents lists available at ScienceDirect

Transportation Research Part D

journal homepage: www.elsevier.com/locate/trd

Impact on flight trajectory characteristics when avoiding the formation of persistent contrails for transatlantic flights

Feijia Yin[a,c,*], Volker Grewe[b,c], Christine Frömming[b], Hiroshi Yamashita[b]

[a] School of Power and Energy, Northwestern Polytechnical University, West Youyi Road 127, Beilin District, Xi'an, Shaanxi 710072, PR China
[b] Deutsches Zentrum für Luft- und Raumfahrt, Institut für Physik der Atmosphäre, Oberpfaffenhofen, Münchener Straße 20, 82234 Weßling, Germany
[c] Faculty of Aerospace Engineering, Delft University of Technology, Kluyverweg 1, 2629 HS Delft, the Netherlands

ARTICLE INFO

Keywords:
Flight trajectory optimization
Contrail avoidance
Seasonal changes in trajectory characteristics

ABSTRACT

This paper studies the impacts on flight trajectories, such as lateral and vertical changes, when avoiding the formation of persistent contrails for transatlantic flights. A sophisticated Earth-System Model (EMAC) coupled with a flight routing submodel (AirTraf) and a contrail submodel (CONTRAIL) is used to optimize flight trajectories concerning the flight time and the flight distance through contrail forming regions (contrail distance). All the trajectories are calculated taking into account the effects of the actual and local meteorological parameters, e.g., wind, temperature, relative humidity, etc. A full-year simulation has been conducted based on a daily flight schedule of 103 transatlantic flights. The trade-off between the flight time and contrail distance shows a large daily variability, meaning for the same increase in flight time, the reduction in contrail distance varies from 20% to 80% depending on the daily meteorological situation. The results confirm that the overall changes in flight trajectories follow a seasonal cycle corresponding to the nature of the potential contrail coverage. In non-summer seasons, the southward and upward shifts of the trajectories are favorable to avoid the contrail formation. In summer, the northward and upward shifts are preferred. A partial mitigation strategy for up to 40% reduction in contrail distance can be achieved throughout all the seasons with a negligible increase in flight time (less than 2%), which represents a reasonable trade-off between flight time increase and contrail avoidance.

1. Introduction

Scientific understanding reveals the unequivocal evidence of climate change due to anthropogenic activities since the mid-20th century (Solomon et al., 2007), and aviation shares 3–5% of the anthropogenic causes to climate change. Nevertheless, the demand for air transportation is anticipated to grow at 4.4% per annum in the next 20 years (Airbus, 2017). In facing the continuing expansion of air traffic, the goal of developing eco-efficient aviation becomes increasingly challenging.

Aircraft emit gases such as carbon dioxides (CO_2), nitrogen oxides (NO_x), water vapor, sulphur oxides (SO_x), and aerosols. The atmospheric feedback to these species, especially non-CO_2 emissions, involves complex physical processes acting on different spatial and temporal scales (Lee et al., 2010). The resulting climate impact differs not only by quantity and by type of emissions but also by altitude, geographical location, time and the local weather conditions. Such complexities make it difficult to reduce the climate

* Corresponding author at: School of Power and Energy, Northwestern Polytechnical University, West Youyi Road 127, Beilin District, Xi'an, Shaanxi 710072, PR China.
E-mail addresses: f.yin@tudelft.nl, feijia.yin@outlook.com (F. Yin).

https://doi.org/10.1016/j.trd.2018.09.017

Available online 02 October 2018

Nomenclature

Abbreviations

ARMOGA	Adaptive Range Multi-objective Genetic Algorithm
BADA	Base of Aircraft Data
PCC	potential contrail coverage
PCCDist	contrail distance [km]
CPs	control points
DJF	December, January and February
DR	distance ratio
EMAC	ECHAM5/MESSy atmospheric chemistry
JJA	June, July and August
MAM	March, April and May
RF	radiative forcing
SAC	Schmidt-Appleman Criterion
SON	September, October and November

Symbols

c_p	specific heat at constant pressure [J/kg/K]
$\Delta\lambda_{airport}$	longitude distance for a given airport pair[km]
α	weight factor
K	coefficient [seconds/km (contrails)]
n	number of waypoints
t	flight time [minute]

Subscripts

dist_opt	maximal contrail distance reduction scenario
t_opt	time optimal scenario
tot	total value

impact of aviation systematically, yet offers mitigation options beyond the sole reduction of emissions, e.g., the optimization of flight trajectories avoiding climate-sensitive regions (Matthes et al., 2017; Rosenow et al., 2017; Lim et al., 2017).

Studies in Lee et al. (2009) and Grewe et al. (2017) show that CO_2 emissions share significantly less than 50% of the total aviation radiative forcing (RF) if non-CO_2 effects from NO_x, water vapor, direct aerosol, contrails and the induced cirrus (contrail-cirrus) are included. Fig. 1 (Grewe et al., 2017) (an update of the Fig. 4 in Lee et al. (2009) shows that the contrail cirrus is the largest individual contributor to the total aviation RF with some uncertainties at the current level of understanding. Due to insufficient knowledge about the aviation induced cirrus, it was not possible to quote a likelihood range with a certain confidence level for the RF of the total contrail cirrus, therefore, only a possible range was given. An identical conclusion is also given in a recent IPCC (Intergovernmental Panel on Climate Change) report (Solomon et al., 2007).

The formation of persistent contrails depends on the environmental conditions and aircraft/engine technologies. The Schmidt-Appleman Criterion (SAC) (Schmidt, 1941; Appleman, 1953) tells that the straightforward technological measure to reduce contrail formation would be reducing the H_2O emission index, increasing the fuel specific heat capacity, or decreasing the propulsion efficiency. Most of them are undesirable for the fuel efficiency of an aircraft. Nevertheless, the technological measures may change the

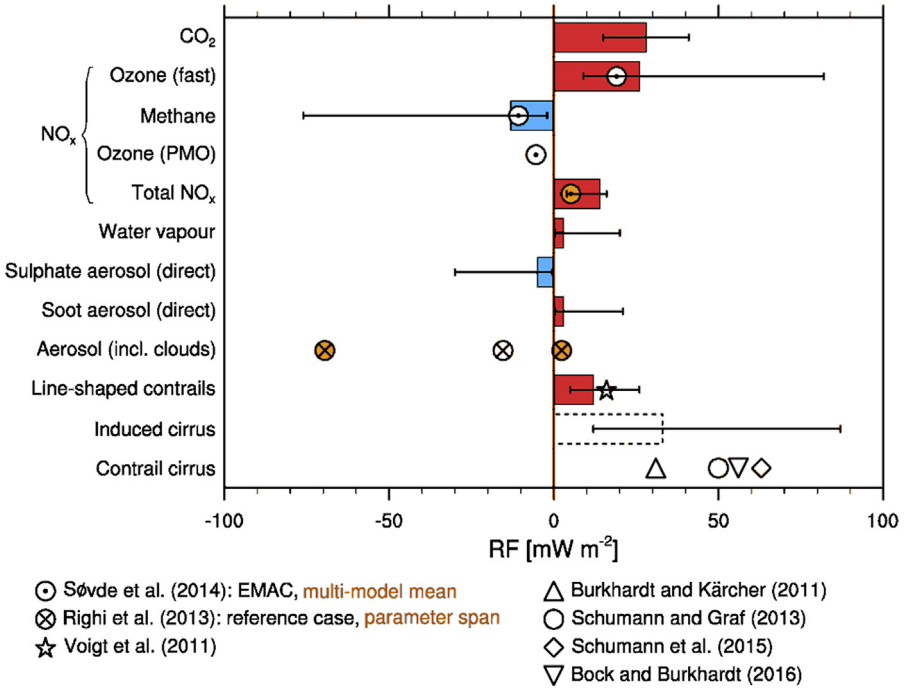

Fig. 1. Aviation induced RF from different components (Grewe et al., 2017; Burkhardt and Kärcher, 2011; Søvde et al., 2014; Voigt et al., 2011; Schumann and Graf, 2013; Bock and Burkhardt, 2016; Righi et al., 2013; Schumann et al., 2015). Error bars represent the 90% likelihood range for each estimate.

contrail composition and properties (e.g., particle number and size, contrail optical thickness, etc.) but not the formation conditions (Gierens et al., 2008). Earlier research has demonstrated the feasibility of changing flight profiles to avoid the contrail formation regions, i.e., the ice-supersaturated and low-temperature regions, hence, reducing contrail occurrence (Mannstein et al., 2005; Sridhar et al., 2011; Chen et al., 2012; Gao and Hansman, 2013). On the other hand, the current flight paths are mainly designed to minimize flight time or fuel cost. Changes in the optimization strategy may provoke time or cost penalties (Campbell et al., 2013; Zou et al., 2016; Hartjes et al., 2016), which have to be shared by different stakeholders and customers. Therefore, tradeoffs have to be estimated in this regard.

In this paper, we aim at investigating the effectiveness of the contrail distance reduction for transatlantic flights and the resulting impact on the flight characteristics. The analysis follows a thorough 4D trajectory optimization approach that incorporates the actual and local weather conditions and the information on potential contrail coverage (PCC). A full year simulation is conducted such that the seasonal cycle of PCC and wind can be reflected. Please note, that within the present study the lifetime and radiative impact of contrails are not included, but only the formation of contrails as a first step.

This paper is organized as follows. In Section 2, the 4D trajectory optimization approach concerning flight time and contrail distance is elaborated. The model consists of an Earth-System model coupled with a 4D trajectory calculation tool (AirTraf) and a PCC prediction submodel (CONTRAIL). Section 3 presents the temporal pattern of the wind fields and PCC predicted from the models in this paper. Section 4 focuses on the trajectory optimization to estimate the tradeoff between flight time and contrail distance on an annual timescale. Based on the optimization results, the effectiveness of the reduction of contrail distance and the consequent changes in flight characteristics are evaluated. In Section 5, general issues are discussed. Finally, conclusions and further plans are provided in Section 6.

2. Air traffic simulation framework for contrail avoidance

2.1. The base model

The base model of the present air traffic simulation is the ECHAM/MESSy Atmospheric Chemistry (EMAC) model. The EMAC model is a numerical chemistry and climate simulation system that includes submodels describing tropospheric and middle atmosphere processes and their interaction with oceans, land and human influences (Jöckel et al., 2010). It uses the second version of the Modular Earth Sub-model System (MESSy2) (Jöckel et al., 2010) to link multi-institutional computer codes. The core atmospheric model is the 5th generation European Centre Hamburg general circulation model (ECHAM5) developed by the Max Planck Institute for Meteorology (Roeckner et al., 2006; Roeckner et al., 2003). For the present study, we applied EMAC (ECHAM5 version 5.3.02, MESSy version 2.52.0) in the T42L31ECMWF-resolution, corresponding to 2.8° by 2.8° in latitude and longitude and 31 vertical hybrid pressure levels up to 10 hPa (an altitude of roughly 30 km). The vertical resolution at flight levels is roughly 1 km. The simulation time step is 12 min. Such a model resolution will provide us with reasonable weather data.

EMAC has been extensively validated with other models, for instance, ACCMIP presented in Lamarque et al. (2013), with respect to atmospheric dynamics, cloud occurrence, chemistry, etc. An overview is given in Jöckel et al. (2016). Here we use the submodels: AirTraf V1.0 (Yamashita et al., 2016) and CONTRAIL V1.0 (supplementary of (Grewe et al., 2014).

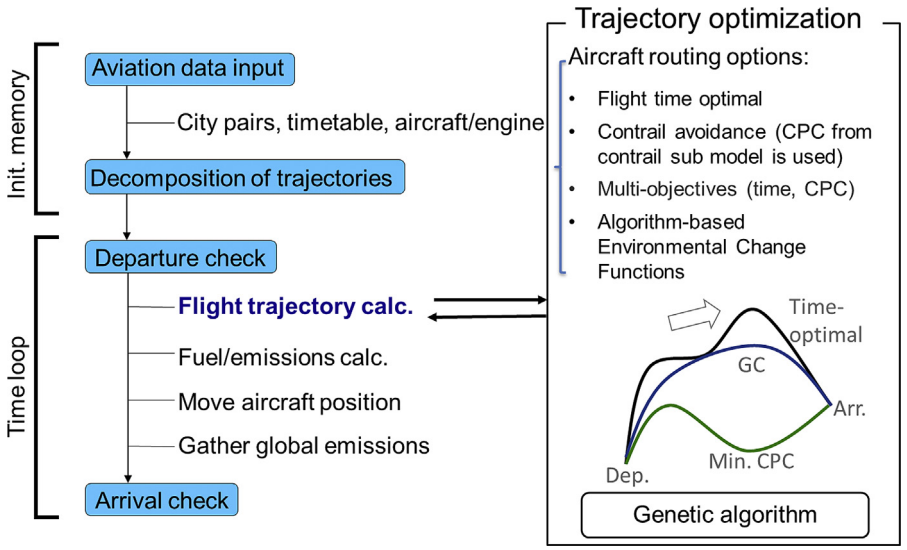

Fig. 2. An overview of the AirTraf simulation tool (Yamashita et al., 2015). CPC stands for potential contrail coverage and GC means great circle.

2.2. The AirTraf submodel

The AirTraf submodel (developed by Yamashita et al. (2016)) is a 4D trajectory simulation tool for global air traffic, including the effects of actual and local weather conditions (pressure, temperature, wind, etc.), changing with the model time step (here 12 min). The unique feature of AirTraf combined with EMAC provides the opportunity to assess the impact of aviation emissions, resulting from aircraft trajectory optimization on the atmospheric composition and RF.

Fig. 2 provides an overview of the AirTraf working principle. At the model initial phase, the air traffic data, including flight schedule and the characteristics of aircraft/engine, is required. The flight schedule contains flight connection information, e.g., the departure/arrival airport codes, the latitude/longitude of airports, and the departure time. An aircraft takes off when it reaches the departure time in the time loop of EMAC. Depending on the routing options, the flight trajectory is calculated. The fuel flow rate and emissions are calculated using the total energy model based on the state-of-art Eurocontrol's Base of Aircraft Data (BADA) method (Eurocontrol, 2011) and the DLR fuel flow method (Deidewig et al., 1996). Though using BADA model might introduce errors in fuel consumption as compared to the manufacture's models, we present mainly relative changes and expect that this minimizes biases in the fuel consumption. The engine performance data is taken from the International Civil Aviation Organization databank (ICAO, 2005).

A flight trajectory is calculated based on a number of waypoints and segments. The output files contain the coordinates of the aircraft (latitude, longitude, and altitude), flight time, flight distance, fuel consumption, emissions, and contrail distance at each waypoint or over a flight segment. The coordinates of each waypoint along the great circle are determined by using Vincenty Formula (Vincenty, 1975) for central angle and the linear interpolation based on polar coordinates for the distance between two neighboring waypoints.

Since the weather conditions, e.g., wind, pressure, etc., are taken from the EMAC grid to the adjacent waypoint, to ensure the accuracy of the weather data, a sufficiently large number of waypoints should be used. A sensitivity study has been performed in this regard by Yamashita et al. (2016), and subsequently, 101 waypoints are selected for all the routing options. Considering the transatlantic flights in this paper, the resolution of the trajectory calculation would be 50–60 km.

Currently, there are following routing options available: great circle (minimum flight distance between the departure airport and the arrival airport on the surface of the Earth), minimum flight time, and minimum contrail distance, while considering actual and local wind. By combining the flight time and contrail distance, the tradeoffs between these two are estimated. The additional options

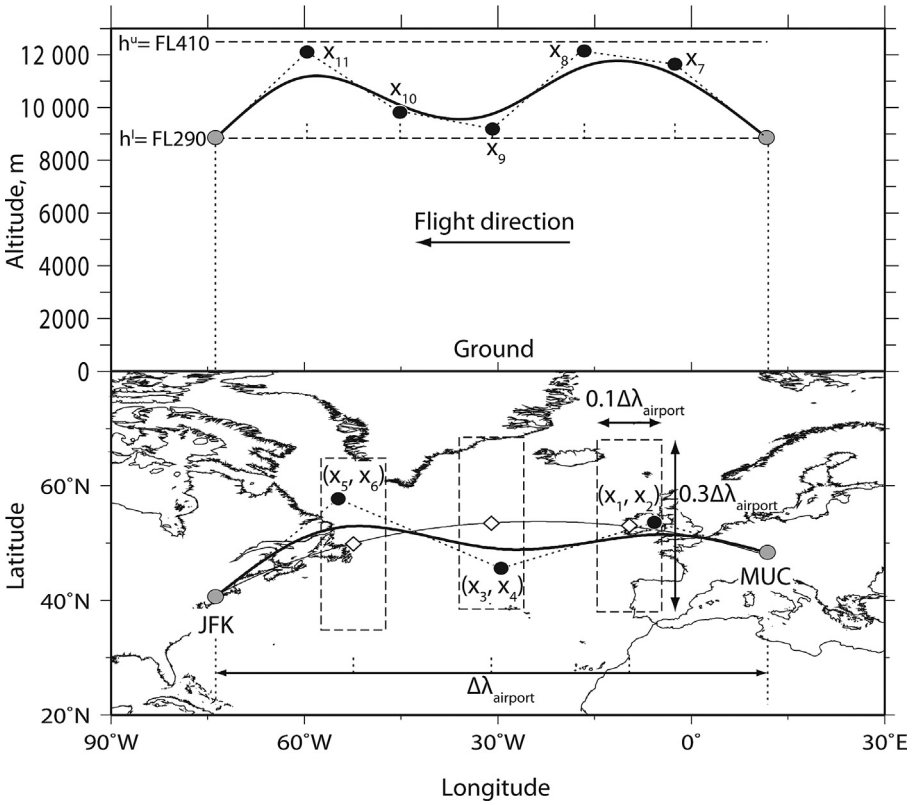

Fig. 3. A demonstration of the geometry definition for a flight trajectory in the vertical cross-section (top) and the projection on the Earth (bottom) (Yamashita et al., 2016). The bold solid line indicates the real trajectory from MUC to JFK. The black dots are control points determined by design variables $x = (x_1, x_2, \cdots x_{11})^T$. Bottom: the dashed boxes show rectangular domains of three control points. The diamonds along the great circle are center points of the boxes. $\Delta\lambda_{airport}$ is the longitude distance between two cities.

including minimum cost and minimum climate impact (the climate impact from a full set emission) will be introduced in the next version of AirTraf. For all routing options, the local weather conditions are obtained from EMAC at each time step of 12 min.

The flight altitudes of great circle routes are assumed to be constant, whereas, the flight altitudes of non-great circle routes change dynamically depending on the optimization routine. The trajectories are optimized using the Adaptive Range Multi-objective Genetic Algorithm (ARMOGA version 1.2.0, (Sasaki et al., 2002; Sasaki and Obayashi, 2005). The Genetic Algorithm (GA) setup, including the generations, individuals, and operators (crossover and mutation), has been thoroughly analyzed (Yamashita et al., 2016). Regarding the optimization constraints, the restrictions for vertical and lateral shifts are considered, but not the other aspects, i.e., conflict avoidance, etc.

Fig. 3 demonstrates the working principle of the trajectory optimization based on an example flight from New York (JFK) to Munich (MUC). The top figure shows the vertical cross section and the bottom figure is the projection on the earth. During the trajectory optimization phase, GA searches the optimal solutions around the great circle of a given city pair. The geographical locations and altitudes of trajectories are adjusted by so-called control points (CPs, black dots in Fig. 3) governed by an array of independent design variables X.

In principle, the more CPs can express the more realistic trajectories, however, the computational load is increased as well. By considering the trade-off between the quality of flight trajectories and the computational load, 8 CPs were selected. These 8 CPs are governed by 11 independent design variables $X = (x_1, x_2, \cdots x_{11})^T$. The lateral changes are realized by 3 CPs governed by the variables (x_1, $x_2 \cdots x_6$), whereas, the vertical changes are realized by 5 CPs governed by (x_7, x_8, $\cdots x_{11}$).

For the lateral changes (bottom), the CPs are movable within three rectangular domains (dashed boxes). The center point (diamonds along the great circle) of each rectangular domain is determined along the great circle by dividing the longitude distance ($\Delta\lambda_{airport}$) between two cities into four equal parts. The domain size is set to $0.1 \times \Delta\lambda_{airport}$ (short side) and $0.3 \times \Delta\lambda_{airport}$ (long side) which defines the upper and lower bounds of the variables x_1, $x_2 \cdots x_6$.

For the vertical changes (top), the CPs are located to divide $\Delta\lambda_{airport}$ into six equal parts. The CPs (x_7, x_8, $\cdots x_{11}$) are moved vertically to change the altitude. The vertical constraint is [FL290, FL410] as indicated by the dashed lines.

To verify the consistency of AirTraf, the simulation results on the flight time, fuel consumption, NO_x emission indices and aircraft weight based on selected city pairs were compared to different literature data obtained under similar conditions (aircraft/engine type, flight conditions, and weather conditions). The flight time was about 0.1% lower compared to the reference data in Sridhar et al. (2014). The difference in fuel consumption was about −1% to −9% compared to the Eurocontrol data (Eurocontrol, 2011) when different weights of the baseline is considered. The difference in EINOx ranged between 5% and 8% compared to the reference data in Jelinek et al. (2004). The verification of aircraft weight is related to that of the fuel use calculation. The analysis confirmed the validity of the results predicted by AirTraf. For the details of the model verification, the readers are referred to the literature (Yamashita et al., 2016).

2.3. The CONTRAIL submodel

The CONTRAIL submodel calculates the potential coverage of persistent contrails instantaneously with the EMAC resolution specified in Section 2.1. The threshold for contrail formation is determined using the SAC thoery. The contrails form when the mixture of engine exhaust and ambient air reaches water saturation at the sufficient low temperature, and they persist when the ambient air is ice-supersaturated (Aircraft Contrails Factsheet, 2000). The parametrization of the SAC is given in Table 1.

Once the contrails are formed, the PCC as the fraction of an EMAC grid box, which can be maximally covered by contrails, is calculated depending on ambient conditions. In the CONTRAIL submodel, the PCC is the difference between the maximum possible coverage of both contrails and cirrus (b_{co+ci}), and the coverage of natural cirrus alone (b_{ci}), as described in Eq. (1).

$$PCC = b_{co+ci} - b_{ci}, \quad \text{with} \tag{1}$$

$$b_{ci} = 1 - \sqrt{\frac{r - r_{ci}}{r_{sat} - r_{ci}}}, \quad \text{and} \tag{2}$$

$$b_{co+ci} = \begin{cases} \frac{r - r_{co}}{r_{sat} - r_{ci}} - b_{ci} \cdot (1 - b_{ci}) & \text{for } r_{co} \le r \le r^* \\ 1 & \text{for } r > r^* \end{cases} \tag{3}$$

With r is the EMAC grid mean relative humidity; r_{ci} and r_{co} are critical relative humidity above which a fraction of EMAC grid box is covered by cirrus and is ice-supersaturated, respectively; r_{sat} is the relative humidity at saturation; The relative humidity $r^* = r_{sat} - (r_{ci} - r_{co})^2 / (r_{sat} - r_{ci})$. Details of the calculations for b_{co+ci} and b_{ci} can be found in Grewe et al. (2014) and its supplementary

Table 1
The parametrization of the SAC in the CONTRAIL submodel.

Parameters	Descriptions	Values	Units
C_p	Specific heat	1004	J/kg/K
EIH_2O	Water emission index	1.25	kg/kg(fuel)
η	Propulsion efficiency	0.31	[-]
Q	Fuel specific heat capacity	43.2	MJ/kg

material therein.

The CONTRAIL modelling approach has been validated in Frömming et al. (2011) with respect to mean ice water content, probability density function (PDF) of the ice water content, PDF of the optical depth in the visible spectrum, longwave and shortwave radiation of high ice clouds, based on the Mhyre Benchmark test (Myhre et al., 2009). The results show a reasonable agreement with other models, satellite and in situ measurement. Contrails are simulated with a higher frequency of lower ice water contents and accordingly higher frequency lower optical thicknesses compared to observational data, which might result either from deficiencies in observational techniques to detect such contrails (e.g. at the end of the contrail's lifetime) or may constitute a model bias.

In addition, Section 3.1 provides the variability of the PCC calculated from the CONTRAIL submodel.

2.4. The contrail distance calculation

For the routing optimization, AirTraf uses the contrail distance instead of the PCC. The contrail distance is the total flight distance through the PCC regions. The flight distance is calculated based on the number of waypoints along a flight profile, the resolution of which differs from the EMAC grid for the PCC calculation. The approach described in Fig. 4 has been adapted to address this issue.

AirTraf first identifies the adjacent EMAC grid box to a waypoint. The PCC calculated within this grid box is then exported to the corresponding waypoint, as demonstrated in the procedure a) of Fig. 4. Afterward, the contrail distance through the i^{th} waypoint ($PCCDist_i$) is derived by multiplying the contrail coverage at the i^{th} waypoint (PCC_i) with the flight distance ($(d_{i-1} + d_i)/2$). This procedure is demonstrated in the subplot (b) of Fig. 4. Note that for the first and the last waypoint, there is only one flight segment associated. Hence, the half-length of the one segment is multiplied by the PCC value.

The total contrail distance for a given flight is then calculated following Eq. (4)

$$PCCDist_{tot} = \sum_{n=1}^{101} PCCDist_{(n)} \tag{4}$$

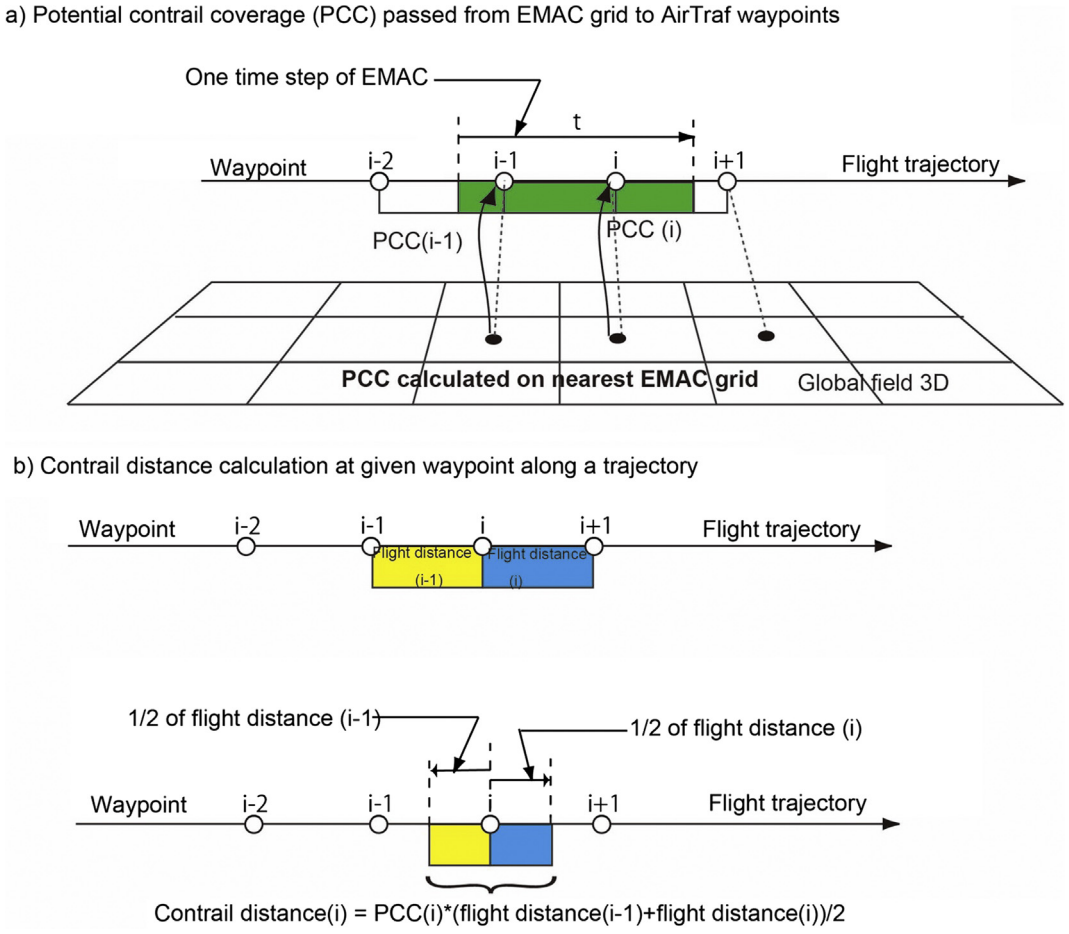

Fig. 4. Illustration of the contrail distance calculation procedure. (a) PCC exported from EMAC grid to waypoints along the trajectories. (b) Contrail distance calculation at a waypoint (i).

With $PCCDist_{(n)}$ is the contrail distance at the n_{th} waypoint; $PCCDist_{tot}$ is the total contrail distance of a given flight.

2.5. The optimization strategy for contrail distance mitigation

The optimization strategy is to mitigate the total contrail distance while minimizing the flight time, which is an essential performance indicator. Eq. (5) defines the objective function,

$$f = (1-\alpha)\cdot t + \alpha\cdot K\cdot PCCDist_{tot} \tag{5}$$

With t is the total flight time; $PCCDist_{tot}$ is the total contrail distance calculated using Eq. (4); K is an index calculated using Eq. (6) with a unit of seconds/km(contrails), which indicates the changes in flight time per unit reduction in the contrail distance; and α is a weight control factor between Solomon et al. (2007) to adjust the contribution of each objective to the total.

$$K = \frac{t_{dist\_opt} - t_{t\_opt}}{PCCDist_{t\_opt} - PCCDist_{dist\_opt}} \tag{6}$$

In Eq. (6), the subscript *dist_opt* represents the minimum contrail distance scenario; and the *t_opt* represents the minimum flight time scenario.

Table 2 provides the trajectory optimization setup used in this paper. We use 103 daily transatlantic flights, amongst which 51 flights are eastbound and 52 flights are westbound. These flights are a subset of daily transatlantic flights from the REACT4C project (http://www.react4c.eu/) (Grewe et al., 2014), which was an EU project to investigate the potential of climate-optimized flight routing to reduce the atmospheric impact of aviation.

To capture the seasonal variability, an annual air traffic simulation is conducted by repeating the daily flight schedule, but with varying meteorology. We use a typical long-range aircraft model with the cruise Mach number of 0.82. Depending on the wind, the ground speed is calculated. The vertical constraints are between FL290 and FL410 (8.9–12.5 km).

By minimizing the objective function in Eq. (5), the tradeoffs between the flight time and the contrail distance are estimated. α is varied from 0 to 1 at a step of 0.2, which defines six optimization scenarios as presented in Table 3. If α equals zero, the minimum flight time is obtained. If α equals one, the optimizer minimizes the contrail distance. Otherwise, the tradeoffs between the contrail distance and flight time are considered.

According to Eq. (5), the index K is required for the partial mitigation of the contrail distance. To calculate K, we first performed two sets of annual simulations using the daily flight schedule in Table 2 concerning the time minimum scenario and the contrail distance minimum scenario, respectively. The flight time and contrail distance for individual flights on each day are then used in Eq. (4) to calculate K. Accordingly we obtain a two-dimensional matrix containing K values as a function of the number of flights and days.

Fig. 5 presents the daily variability of the fleet averaged K value. We found that the impact on flight time per km reduction in contrail distance varies from zero to more than a few minutes. We performed a sensitivity study to evaluate the impact of K values on the optimization results. The analysis showed that changing the K value affects the location of a specific dataset along the Pareto Front, but not the overall shape. Hence, the averaged K values, 1.7 min/km for summer and 1 min/km for non-summer, are used in the optimization. The definition of each season is given in Table 4 and is used throughout this paper.

3. The validity of the calculated potential contrail coverage and wind field

This section presents the temporal pattern of potential contrail coverage and wind field predicted by the EMAC model.

3.1. The temporal change in potential contrail coverage

The PCC over a full year (2011) is simulated using EMAC with the CONTRAIL submodel as described in Section 2.3. In Fig. 6, the zonal mean PCC in winter (left) and summer (right) are presented. In each figure, the region confined by the dashed lines represents the vertical constraints used in AirTraf for this paper.

Fig. 6 shows that the calculated PCC follows the pronounced seasonal patterns at middle and higher latitudes, which matches well the results presented in Fichter et al. (2005). In the northern hemisphere, the contrail coverage, especially its vertical span, at the mid-latitudes and the polar region, is larger in winter than summer, which indicates the contrail formation would be more frequent in

Table 2
Trajectory optimization setup.

Elements	Descriptions
Flight schedule	103 transatlantic flights (51 eastbound/52 westbound)
EMAC resolution	T42L31ECMWF (2.8° × 2.8° in latitude and longitude, 31 vertical pressure levels up to 10 hPa, time step 12 min)
Simulation Period	January 2011-December 2011
Altitude constrains	[FL290, FL410]/[8850 m,12500 m]
Mach number	0.82

Table 3
The optimization scenario for given α value.

α value	0	0.2	0.4	0.6	0.8	1.0
Scenarios	Minimum time	Dist_PCC_0.2	Dist_PCC_0.4	Dist_PCC_0.6	Dist_PCC_0.8	Minimum contrail distance

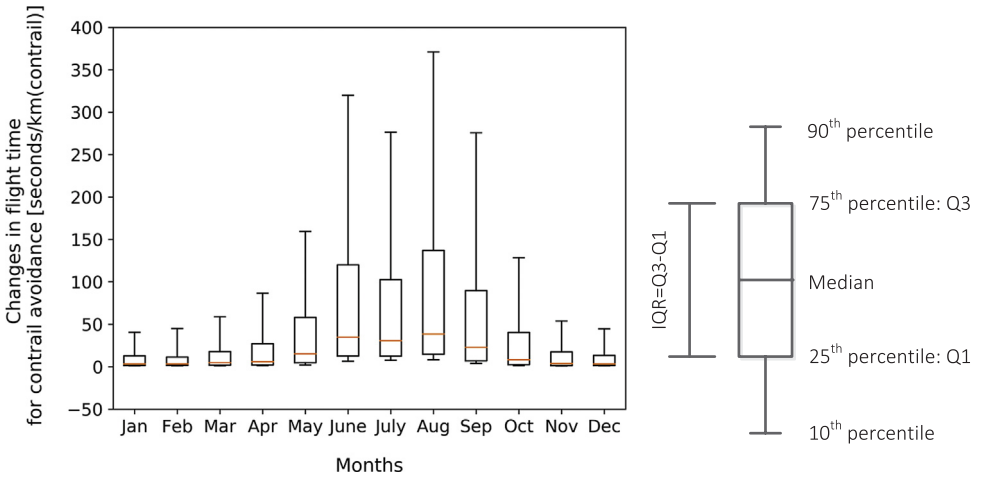

Fig. 5. Seasonal cycle of the daily variability of fleet averaged K values (left) and the explanation of the boxplot (right). For the boxplot: the lower quartile (Q1) is 25%; the upper quartile (Q3) is 75%; the lower whisker is 10%, and the upper whisker is 90%.

Table 4
Seasonal definitions.

Seasons	Months	Abbreviation
Winter	December-January-February	DJF
Spring	March-April-May	MAM
Summer	June-July-August	JJA
Autumn	September-October-November	SON

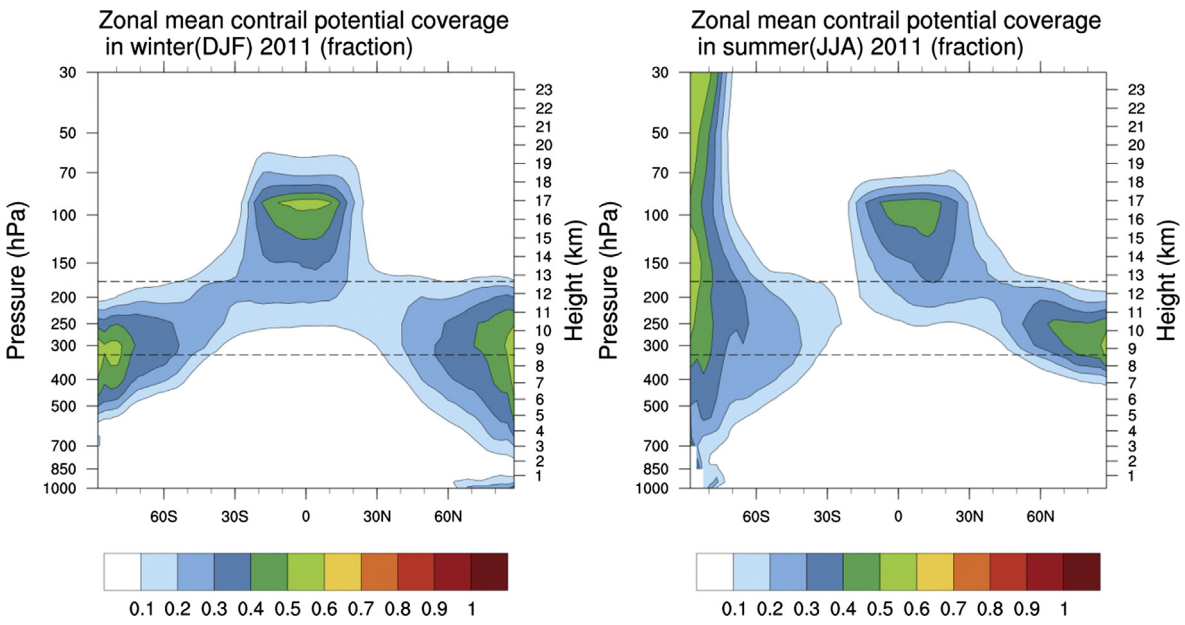

Fig. 6. Zonal mean potential coverage of persistent contrails in winter (left) and summer (right).

winter. Furthermore, at the sub-tropics (around 30°N) in winter, the PCC reduces to a minimal value. This variation trend is mainly because of the troposphere-stratosphere exchange. The interaction of the stratosphere circulation with the troposphere circulation brings the stratospheric warm and dry air into the troposphere in the sub-tropics (Danielsen, 1968), hence reduces the chance for contrail formation in this region. Such exchange effects are much stronger in DJF on the northern hemisphere (škerlak et al., 2015). At the equator, due to the upward motion, there is a large possibility to form contrails in both seasons. As the climatological condition changes with seasonal cycle, in JJA the interference by stratospheric circulation becomes stronger in the southern hemisphere. Hence, in JJA, the minimal PCC occurs at the southern sub-tropics.

Based on the contrail formation pattern, both vertical and latitudinal changes will be expected when avoiding the contrail formation regions, for the transatlantic flights studied in this paper. The other condition with a strong influence on the optimization results is the wind pattern, which will be presented in the next section.

3.2. The temporal change in the wind field

Wind fields are calculated in EMAC by solving the primitive equations. The mean values of the zonal wind in DJF and JJA are presented in Fig. 7. Again, the dashed lines indicate the vertical constraints for the AirTraf optimization. The negative sign indicates the east wind, and the positive sign indicates west wind.

From Fig. 7, we can see a clear seasonal pattern for the westerlies in the subtropics and mid-latitude regions, which are driven by the general circulation. In the northern hemisphere, the wind speed is much stronger in winter than in summer. Therefore, the eastbound flights will benefit more from tailwinds.

4. Trajectory optimization for contrail avoidance

In this section, the results of the trajectory optimization are analyzed. Firstly, a sensitivity analysis is performed concerning the contrail distance of the minimum time flights (the baseline of the current study). Section 4.2 presents a case study to demonstrate the detouring approach in AirTraf. In Section 4.3, the analysis focuses on the daily variability of flight trajectories based on the overall fleet. The tradeoffs between flight time and contrail distance are studied. The subsequent impacts on flight characteristics are evaluated.

4.1. The temporal change in contrail distance of the minimum time flights

The seasonal variation of the contrail distance is analyzed based on the minimum flight time scenario. The total contrail distance ($PCCDist_{tot}$) is normalized with respect to total flight distance ($Dist_{tot}$) to obtain the distance ratio *(DR)*, as defined by Eq. (7).

$$DR = \frac{PCCDist_{tot}}{Dist_{tot}} \tag{7}$$

Fig. 8 presents the seasonal cycle of the DR for each month the day-to-day variability for the whole fleet using boxplots. Each box contains the daily fleet averaged DRs within a month. The same boxplot definition as in Fig. 5 (right) is applied. The variations of the

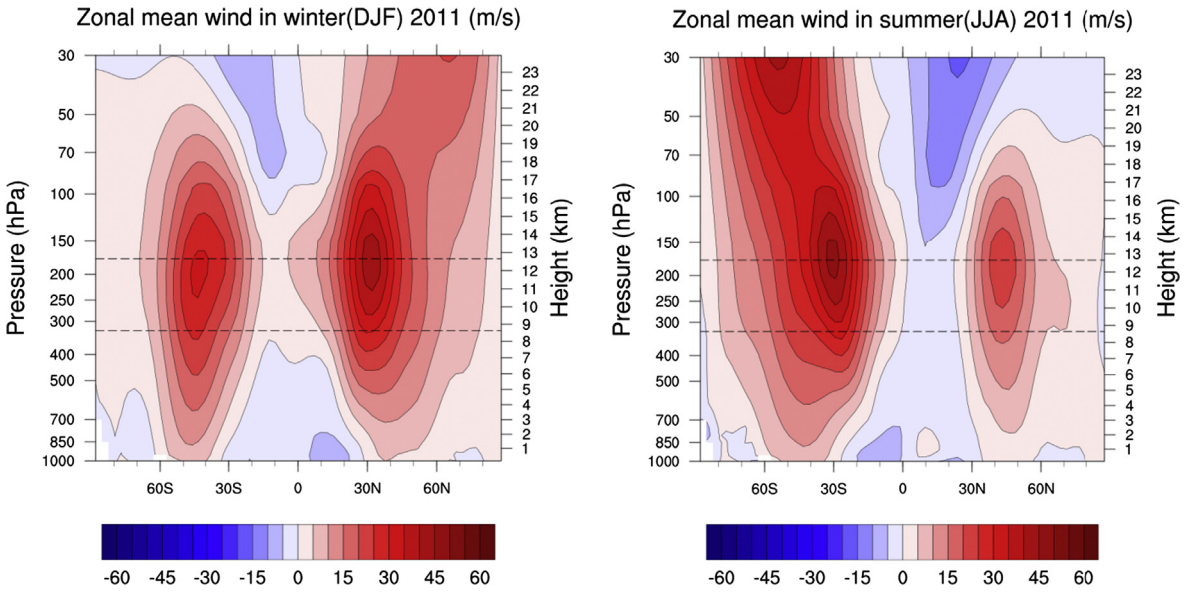

Fig. 7. Zonal mean wind speed in m/s in winter (left) and summer (right); negative sign: east wind and positive sign: west wind.

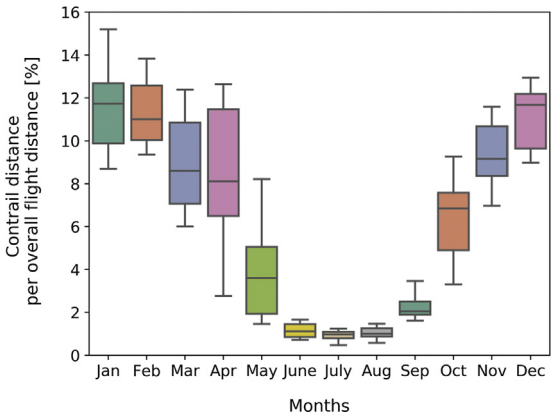

Fig. 8. Seasonal cycle of the daily variability of the contrail distance ratio over one year for the time optimal scenario. The variation in contrail fraction and the daily variability within a month depends solely on the meteorological data. The boxplot definition is the same as in Fig. 5.

contrail distance follow a strong seasonal cycle, which is corresponding to the changes in contrail coverage. In summer, the temperature is high and the relative humidity is low, which is not favorable for contrail formation. Therefore, in June, July, and August, less than 3% of total flight distance may form persistent contrails. In winter, the contrail distance increases substantially, up to more than 10% of the total flight distance. From winter to summer, the contrail distance decreases successively. Furthermore, we see a large daily variability in contrail coverage in non-summer months.

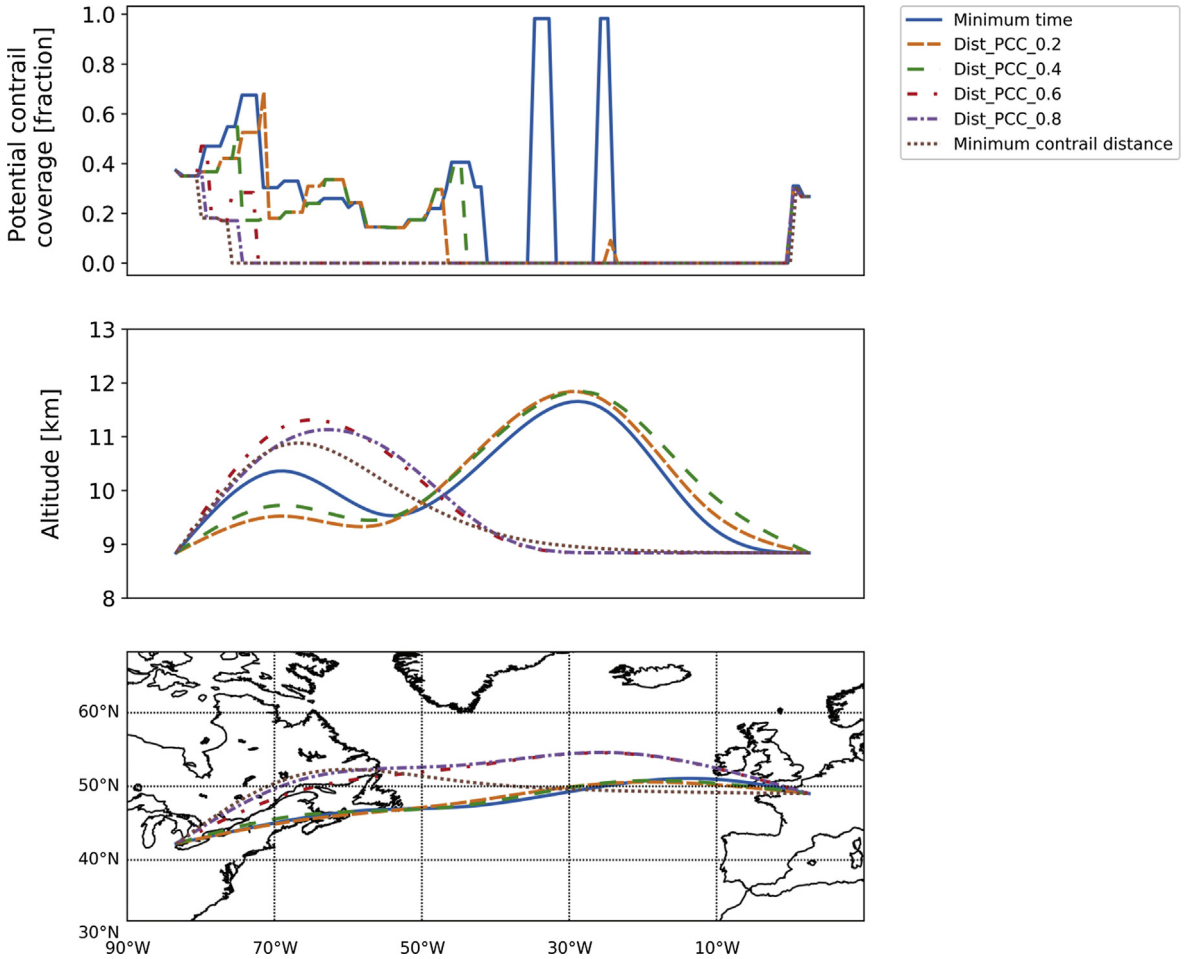

Fig. 9. Flight trajectories corresponding to various optimization objectives defined in Table 3 on 6 January 2011; potential contrail coverage in fraction (top); flight altitude in km (middle); geographical location (bottom); Three plots share the same x-axis as indicated in the bottom figure.

4.2. The case study of a single city pair optimization

To evaluate the effectiveness of the detouring approach, the changes in contrail coverage concerning different optimization scenarios are presented. An example flight from Detroit to Paris is discussed in this section for an individual day and for a whole year.

4.2.1. The one-day simulation results

In Fig. 9, the optimized routes concerning different tradeoffs on an arbitrary day (6 January 2011) are presented. From "Dist_PCC_0.2" to "Dist_PCC_0.8", the contrail distance reduces successively until the maximal reduction in contrail distance is achieved (contrail distance optimal). Flight altitude (middle) and the contrail coverage (top, ranging from Solomon et al. (2007)) are shown together with a geographical projection (bottom) sharing the same x-axis given in the bottom. The top figure shows that nearly the first half of the time optimal flight passes through a contrail formation region and two large peaks occur in the middle of the flight. To avoid those regions, the flight is detoured to either north or to different flight altitudes. By doing so, the contrail distance decreases at the expense of increasing flight time and fuel consumption, which are summarized in Table 5.

Compared to the time optimal flight, the maximal reduction in contrail distance is 84% with an increase in flight time by 7.5% and fuel consumption by 14%. Whereas, a partial mitigation of contrail distance by 42% (Dist_PCC_0.4) only causes a 0.7% increase in flight time and a 0.2% increase in fuel consumption.

4.2.2. The annual simulation results

For the same route from Detroit to Paris, the daily changes in flight time and contrail throughout the whole year are discussed in this section. The time optimal flights are the baseline. The monthly mean values are shown in Fig. 10.

We can see that in the non-summer months, a significant reduction (more than 50%) in contrail distance can be achieved by allowing only less than 2% increase in flight time. In summer, the reduction in contrail distance is less effective since the contrail coverage is already low. Furthermore, the maximal reduction in contrail distance varies from month to month with an increase in flight time from 6% to 12%. Due to the optimization constraints, the maximal reduction rate of contrail distance is less than 90%.

4.3. Fleet optimization for contrail avoidance

The results above (Section 4.2) are for a single city pair on a single day and for monthly means representing a seasonal cycle. In this section, the annual simulation results of tradeoffs on flight time and contrail distance for the 103 daily transatlantic flights are presented.

4.3.1. The variability of Pareto front

Fig. 11 shows the daily variability of the changes in flight time (y-axis) and contrail distance (x-axis) of the whole fleet. Each color-coded area contains the minimum and maximum reduction of contrail distance related to a certain reduction of flight time averaged over the fleet on a daily basis within the same season. The coordinate (0, 0) is the baseline, i.e., the time optimal flights.

The figure shows a large variability in the achievable reduction of contrail distance between each season as well as within a specific season, e.g., by allowing 2% increase in flight time, the contrail distance is reduced by 20–90% depending on the season. The largest variability occurs in summer, where the reduction in contrail distance is less effective than the other seasons. An overview of the flight time increase versus the contrail distance reduction in each season is provided in Table 6.

4.3.2. The changes in flight trajectories

Fig. 11 shows a large discrepancy of changes in contrail distance between winter and summer, requiring a closer look at the trajectory changes, i.e., the flight altitude and geographical location.

In Figs. 12 and 13, the latitudinal and vertical shifts of trajectories over the entire year are presented in the form of the boxplot (inner figure) combined with the kernel density estimates (KDE, outer lines). The changes are relative to the time optimal flights. The daily fleet averaged values for each season are presented. The boxplot follows the same definition as in Fig. 6 (quartile 25th/75th). In each season, there are five plots, corresponding to different reduction rates in contrail distance controlled by the weight factor (α).

From Fig. 12, we can see that in the non-summer seasons, for contrail avoidance, the seasonal changes in latitude follow a similar distribution pattern with the mean value shifts progressively towards the south. The exception happens to the contrail distance

Table 5
Changes in flight characteristics for a flight from Detroit to Paris on January 6th, 2011 to achieve different reductions of contrail distance. The baseline is the time minimum flight.

	Flight time	Flight distance	Contrail distance	Fuel consumption
Time minimum flights (baseline)	6.97 h	6561 km	1484 km	38.4 tons
Dist_PCC_0.2	+0.6%	−0.3%	−37%	+2%
Dist_PCC_0.4	+0.7%	−0.2%	−42%	+0.2%
Dist_PCC_0.6	+1.1%	−2%	−72%	+6%
Dist_PCC_0.8	+2.2%	−2%	−81%	+8%
Contrail distance minimum flights	+7.5%	+0.6%	−84%	+14%

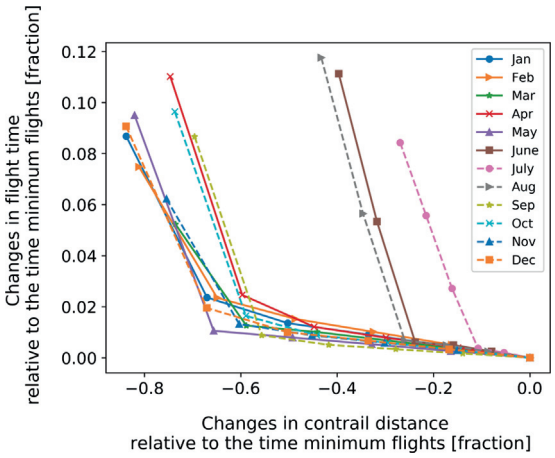

Fig. 10. Tradeoffs between the flight time and contrail distance for flights from Detroit to Paris. Changes are presented relative to the time minimum flights (the coordinate is (0, 0)).

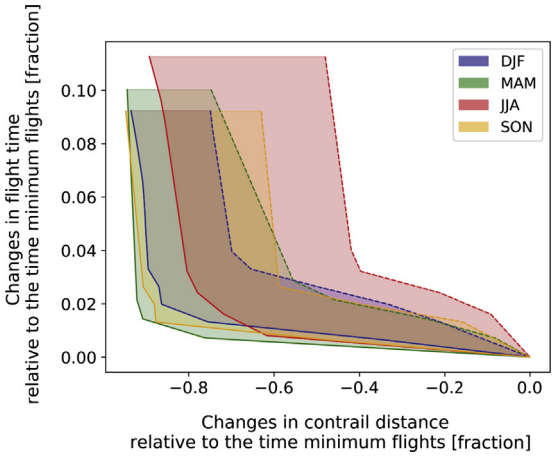

Fig. 11. Tradeoffs between the contrail distance and flight time considering the seasonal variability. The baseline is the time minimum flights (coordinate (0, 0)). The dashed and solid curves indicate the minimum and maximum reduction in contrail distance with each season, respectively.

Table 6
Relative reduction in contrail distance at the expense of the time increase in different seasons given as minimum-maximum ranges; the baseline is the time minimum flights.

Time increase [%]	Contrail distance reduction [%]			
	DJF	MAM	JJA	SON
2	[30,85]	[40,90]	[20,78]	[40,90]
4	[70,87]	[61,92]	[42,81]	[60,91]
6	[72,88]	[63,93]	[45,83]	[62,92]
8	[73,89]	[70,93]	[48,85]	[63,93]
10	N. A.	[75,94]	[50,88]	N. A

optimal flights, for which, the flight shifts northward again, and the deviation increases implying a larger variability. The variations correspond to the zonal mean potential contrail coverage in Fig. 6 and the zonal mean wind speed in Fig. 7. In those maps, we see that flying southwards reduces the contrail coverage as well as experiencing stronger tailwinds, which is beneficial for flight time. However, in summer, the flights shift more to the north, which is opposite to the non-summer seasons.

Fig. 13 shows the vertical changes. For the partial mitigation of contrails, the flight altitude shows a slight increase. As the contrail distance is reduced further, the vertical change remains nearly identical. Whereas for contrail optimal scenario, the flight altitude increases significantly by 0.6–1 km until it reaches the uppermost troposphere to the lowermost stratosphere, where the air is dry hence minimal possibility of forming contrails.

The probability distribution of the flight altitude and latitude on each day in winter and summer are presented in Fig. 14 and

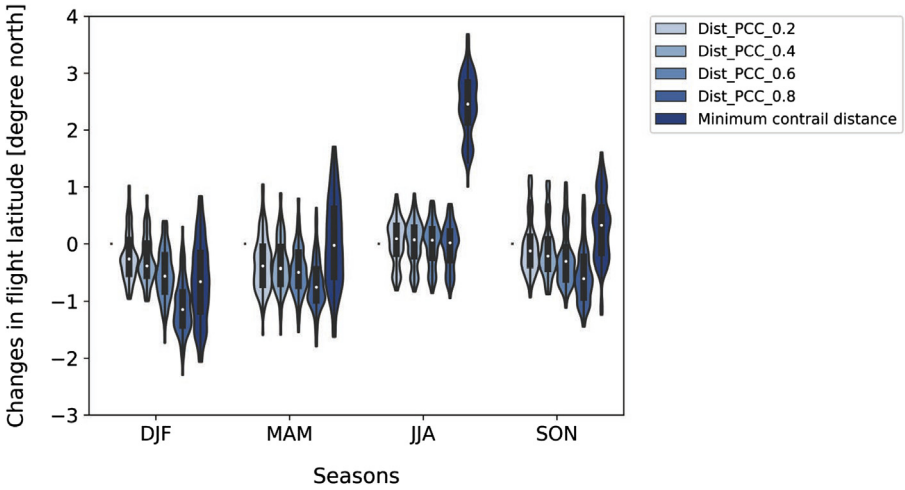

Fig. 12. Change in latitude relative to the minimum time flights in each season; the inner figure is boxplot as defined in Fig. 5; the outer line is the kernel density estimates with the bandwidth of 0.25.

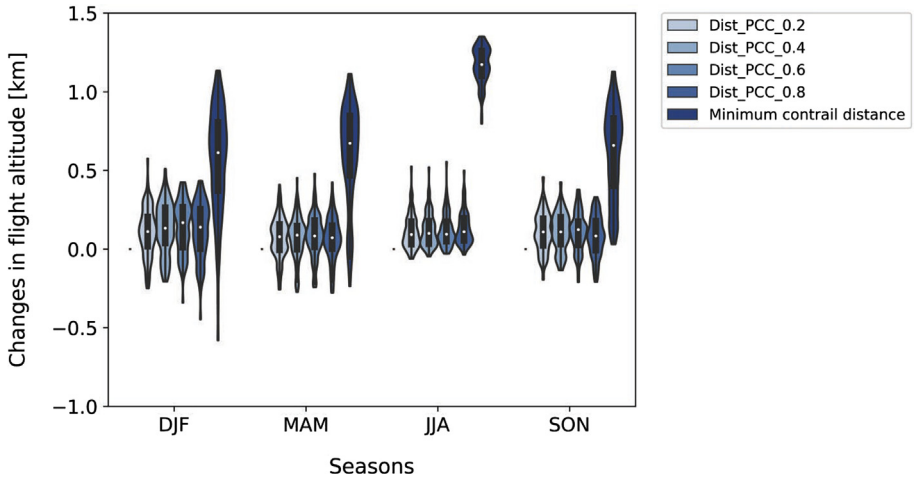

Fig. 13. Changes in flight altitude relative to the minimum time flights; the inner part is the boxplot as defined in Fig. 5; the outer line is the kernel density estimates with the bandwidth of 0.25.

Fig. 15 respectively. Fig. 14 shows that the time optimal flight prefers lower altitudes compared with the contrail avoidance flights. For the maximum reduction in contrail distance, the mean flight altitude increases by approximately 1.5 km compared to the time optimal flights. As for the changes of latitude, a large number of time optimal flights are distributed at around 51° north. To reduce contrails, most flights are relocated more southwards than northwards.

In summer (Fig. 15), the overall flight altitude increases to avoid contrail formation, which is similar to the tendency in winter. The variability of the altitude in summer is smaller than in winter. The latitudinal changes to reduce the contrails can be either south or northwards except for the contrail optimal flights, where flights are shifted northwards.

4.3.3. The impact on flight characteristics

The impacts on flight time, contrail distance, flight distance and fuel consumption for contrail avoidance are presented in Figs. 16–19, respectively. The baseline is the minimum time scenario.

From Figs. 16 and 17, we can see that partial mitigation in contrail distance from 20% to 80% in different seasons results in an increase of flight time by approximately 2%, which corresponds to the large variability indicated by the Pareto front shown in Fig. 11. Any further reduction in contrail distance beyond 60% would cause a step increase in flight time by almost 10%.

Furthermore, Fig. 17 shows that 100% reduction is not feasible since not all areas of potential contrail coverage can be avoided. Note that for the last optimization step for contrail avoidance (from alpha = 0.8–1.0), only a small further reduction of 5–10% in contrail distance is achieved, whereas, flight time and other characteristics are changed dramatically.

Fig. 18 shows the increase in flight distance. For the contrail avoidance scenarios, the flight altitude increases. Since the flight distance depends on the geographical location and the altitude, as explained in Section 2.2, increasing the flight altitude causes an

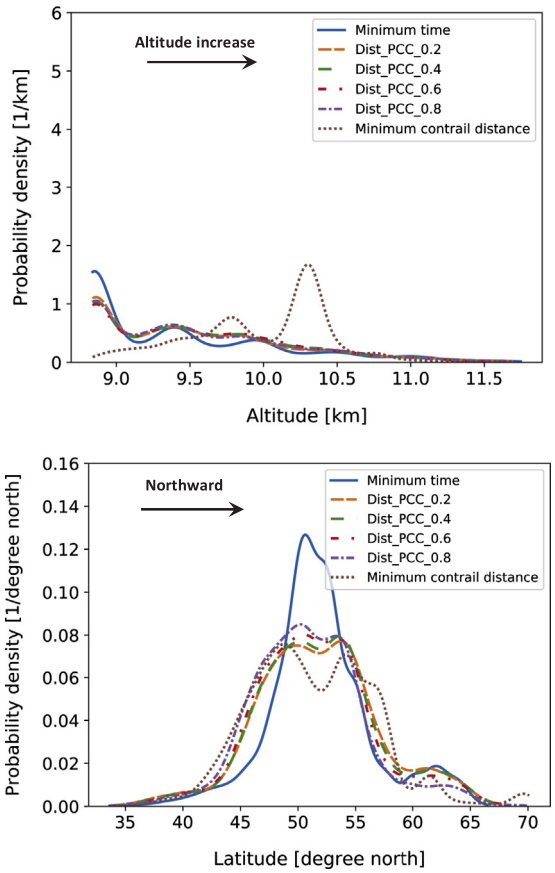

Fig. 14. Probability density distribution of altitude and latitude in winter: altitude (top), latitude (bottom).

increase in flight distance. For the maximum contrail reduction, the flight distance increases by about 6% as shown in Fig. 18.

Fig. 19 shows the impact on fuel burn on the contrail avoidance scenarios. The total fuel burn increases as the contrail distance decrease, with two exceptions: (1) in winter, the fuel consumption of the "Dist_PCC_0.4" case is lower than that of the "Dist_PCC_0.2" case; (2) in summer, the fuel burn of the minimum contrail distance flights reduces. The reason for these two exceptions is mainly due to the increase in flight altitude (Fig. 15), which is beneficial for fuel consumption because of reduced drag at higher altitudes. Even though the flight time increases slightly, the contribution of the altitude change to the fuel burn is more dominant.

5. Discussions

The current trajectory optimization approach is based on contrail distance versus flight time. When taking time-optimal as the baseline case, our results show a clear preference of locally flying at higher altitudes for contrail avoidance. We expect that the results obtained in this study might be different if cost-optimal flights were taken as a base case; a cost-optimal flight would already prefer higher altitudes to reduce fuel consumption. It is likely that, e.g., altitude variations will show a more complex picture, with large variations in upward and downward flight altitude changes. Further analysis will be conducted, with the cost-optimal flight as a baseline, for a full comparison between the two scenarios.

Nevertheless, compared to other studies (Sridhar et al., 2011; Sridhar and Chen, 2010), the present one shows similar results in the effectiveness of contrail avoidance via trajectory optimization approach. Sridhar and Chen (Sridhar and Chen, 2010) investigated a one-day (1 August 2007) air traffic sample for the United States and found that 53% of the contrails could have been avoided with an increase in fuel consumption of around 3%. A more eco-efficient situation was found for a reduction in contrail formation of 35% and a cost increase of only 0.23%.

Still, the question arises whether flying at higher or lower altitudes may be more beneficial to reduce the overall climate impact of aviation. Interestingly, a systematic analysis seems to prevail in studies analyzing the relationship between flight level changes and contrail avoidance. In those studies (Dahlmann et al., 2016; Grewe et al., 2017; Frömming et al., 2012), where only flight altitudes are allowed to change for the whole trajectory, a reduction in contrail occurrence is found for lower altitudes. However, if more flexible trajectories are considered in the optimization, i.e., altitude changes might occur only for a short flight segment, then an increase in flight altitude is beneficial for some routes (Grewe et al., 2017; Schumann et al., 2011; Lührs et al., 2016) and might occur as often as downward shifts (Schumann et al., 2011).

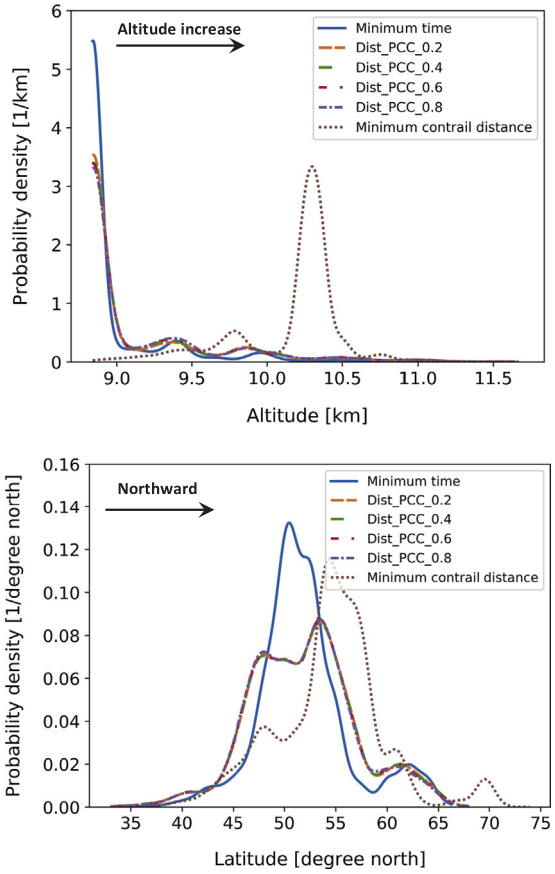

Fig. 15. Probability density distribution of latitude and altitude in summer: altitude (top), latitude (bottom).

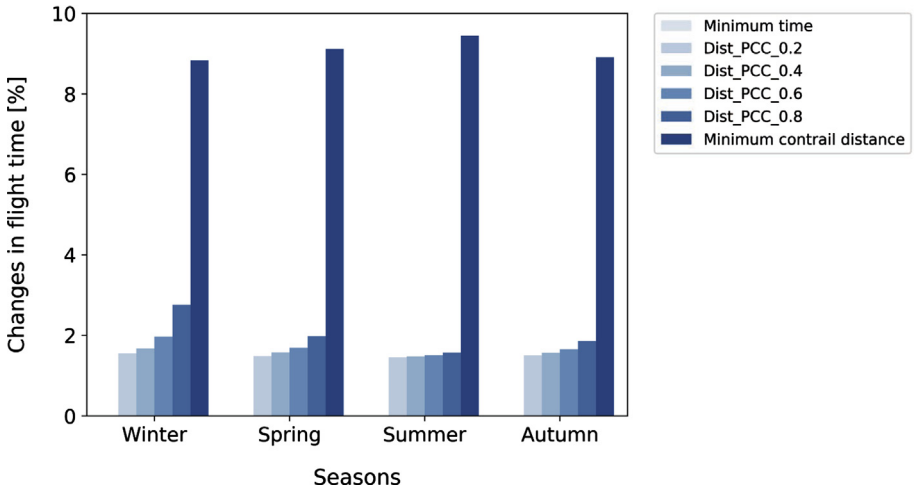

Fig. 16. Changes in total flight time along the Pareto Front. The baseline is the minimum time scenario.

It is important to note that here we were analyzing contrail occurrence, only. The ultimate point of interest is the reduction in the climate impact of aviation and the role of contrail occurrence is only one part, though an important one. Contrail RF consists of a negative shortwave and a positive longwave component. The overall magnitude and sign of contrail RF depend on the amount of contrail cover, its lifetime, particle size and shape, appearance during daytime/nighttime, natural clouds above or below the contrails, and surface properties (Meerkötter et al., 1999). On average, contrails warm the climate (Lee et al., 2009) and (Rap et al., 2010). However, during daytime and especially close to sunset, the cooling mechanism of contrails by scattering sunlight might even be larger than the warming thermal effect for some individual contrails (Schumann et al., 2011; Myhre and Stordal, 2001; Stuber

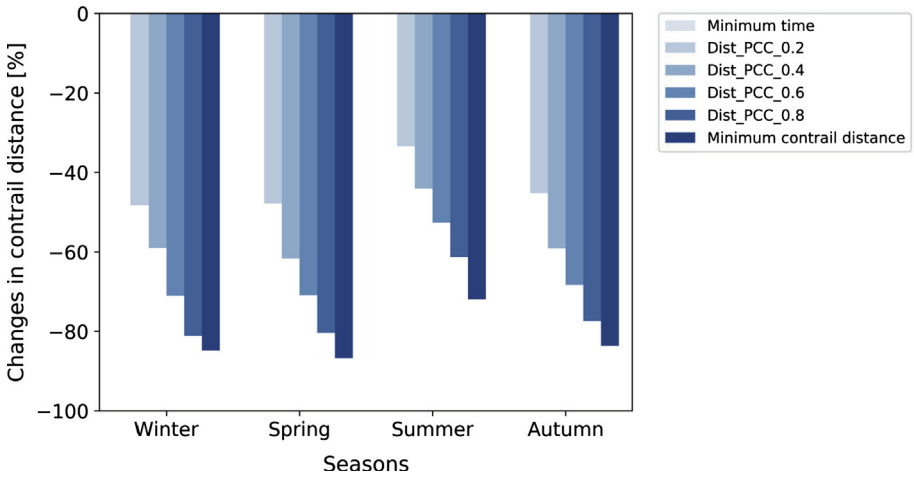

Fig. 17. Changes in total contrail distance along the Pareto Front. The baseline is the minimum time scenario.

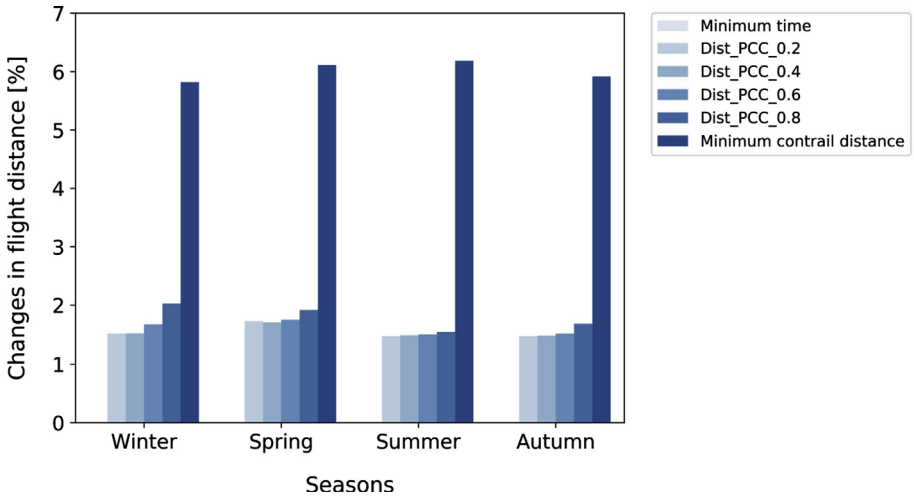

Fig. 18. Changes in total flight distance along the Pareto Front. The baseline is the minimum time scenario.

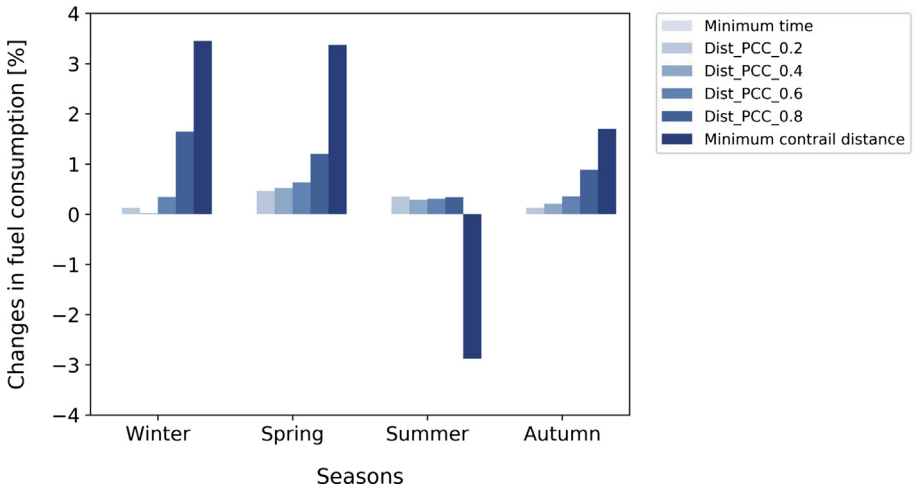

Fig. 19. Changes in total fuel consumption along the Pareto Front. The baseline is the minimum time scenario.

et al., 2006; Grewe et al., 2014; Haywood et al., 2009). Moreover, contrails are not the only climate impact of aviation, other effects arising from, e.g., nitrogen oxide, water vapor, and particulate emissions have to be regarded too, to eventually reduce the overall climate impact from aviation by taking routing changes into account (Grewe et al., 2017). Here, especially water vapor and nitrogen oxide emissions may significantly reduce the benefits from contrail avoidance, when flying at higher altitudes (Frömming et al., 2012; Köhler et al., 2008).

6. Conclusions and future work

This paper focuses on the trajectory optimization with respect to contrail avoidance and the associated changes in flight trajectories. Using an Earth-System Model coupled with a trajectory calculation tool and a contrail calculation model, the trade-off between flight time and contrail distance for transatlantic flights is estimated. Based on the simulation results, the conclusions are drawn as below.

- The seasonal variation of contrail coverage and wind fields is propagated to the changes of the flight routes for the avoidance of contrails.
- In non-summer, the flights shift southwards to avoid the contrail formation regions, whereas, in summer, either southward or northward changes are possible depending on the geographical location. Moreover, increasing the flight altitude is always beneficial to reduce the contrail distance.
- There is a large variability in the tradeoffs between the flight time and contrail distance. For the same increase in flight time, e.g., 2% increase, the reduction in contrail distance varies from 20% to more than 80%. The optimization is less effective in summer than in winter.
- The more eco-efficient approach is to reduce the contrail distance partially with the smallest possible time increase.
- A reduction in contrail distance by 90% causes an increase in fuel consumption by maximal 2.5% in autumn and 4% in winter. Whereas, in summer, maximal mitigation in contrail formation reduces the fuel consumption by 3% though flight time increases by nearly 10%.

This study shows the variation trend of the flight characteristics for contrail avoidance when the different meteorological situations are involved. Further studies on the tradeoff between flight cost (time-related and fuel-related) and the climate impact (consider the full set effects from CO_2, NO_x, water vapor and contrails) concerning actual meteorological situations will be performed. The associated impact on the flight characteristics will be analyzed.

Acknowledgments

This study is supported by the ATM4E project. This project has received funding from the SESAR Joint Undertaking under grant agreement no. 699395 under European Union's Horizon 2020 research and innovation program.

References

Solomon, S., Qin, D., Manning, M., Chen, Z., Marquis, M., Averyt, K.B., Tignor, M., Miller, H.L., 2007. Contribution of working group I to the fourth assessment report of the intergovernmental panel on climate change, 2007. Secondary Contribution of Working Group I to the Fourth Assessment Report of the Intergovernmental Panel on Climate Change, IPCC, 2007. C.U. Press, Cambridge, UK and New York, NY, USA.

Airbus, 2017. Growing Horizons 2017/2036. Secondary Growing Horizons 2017/2036. Airbus, Toulouse, France.

Lee, D.S., Pitari, G., Grewe, V., Gierens, K., Penner, J.E., Petzold, A., Prather, M.J., Schumann, U., Bais, A., Berntsen, T., Iachetti, D., Lim, L.L., Sausen, R., 2010. Transport impacts on atmosphere and climate: Aviation. Atmos. Environ. 44 (37), 4678–4734. https://doi.org/10.1016/j.atmosenv.2009.06.005.

Matthes, S., Grewe, V., Dahlmann, K., Frömming, C., Irvine, E., Lim, L., Linke, F., Lührs, B., Owen, B., Shine, K., Stromatas, S., Yamashita, H., Yin, F., 2017. A concept for multi-criteria environmental assessment of aircraft trajectories. Aerospace 4 (3), 42. https://doi.org/10.3390/aerospace4030042.

Rosenow, J., Förster, S., Lindner, M., Fricke, H., 2017. Impact of multi-critica optimized trajectories on european air traffic density, efficiency and the environment. 12th USA/Europe Air Traffic Management Research and Development Seminar (ATM2017), Seattle.

Lim, Y., Gardi, A., Sabatini, R., 2017. Optimal aircraft trajectories to minimize the radiative impact of contrails and CO_2. Energy Proc. 110, 446–452. https://doi.org/10.1016/j.egypro.2017.03.167.

Lee, D.S., Fahey, D.W., Forster, P.M., Newton, P.J., Wit, R.C.N., Lim, L.L., Owen, B., Sausen, R., 2009. Aviation and global climate change in the 21st century. Atmos. Environ. 43 (22–23), 3520–3537. https://doi.org/10.1016/j.atmosenv.2009.04.024.

Grewe, V., Dahlmann, K., Flink, J., Frömming, C., Ghosh, R., Gierens, K., Heller, R., Hendricks, J., Jöckel, P., Kaufmann, S., Kölker, K., Linke, F., Luchkova, T., Lührs, B., Van Manen, J., Matthes, S., Minikin, A., Niklaß, M., Plohr, M., Righi, M., Rosanka, S., Schmitt, A., Schumann, U., Terekhov, I., Unterstrasser, S., Vázquez-Navarro, M., Voigt, C., Wicke, K., Yamashita, H., Zahn, A., Ziereis, H., 2017. Mitigating the climate impact from aviation: achievements and results of the DLR WeCare project. Aerospace 4 (3), 1–34.

Burkhardt, U., Kärcher, B., 2011. Global radiative forcing from contrail cirrus. Nat. Clim. Change 1, 54. https://doi.org/10.1038/nclimate1068.

Søvde, O.A., Matthes, S., Skowron, A., Iachetti, D., Lim, L., Owen, B., Hodnebrog, Ø., Di Genova, G., Pitari, G., Lee, D.S., Myhre, G., Isaksen, I.S.A., 2014. Aircraft emission mitigation by changing route altitude: a multi-model estimate of aircraft NOx emission impact on O3 photochemistry. Atmos. Environ. 95, 468–479. https://doi.org/10.1016/j.atmosenv.2014.06.049.

Voigt, C., Schumann, U., Jessberger, P., Jurkat, T., Petzold, A., Gayet, J.F., Krämer, M., Thornberry, T., Fahey, D.W., 2011. Extinction and optical depth of contrails. Geophys. Res. Lett. 38 (11). https://doi.org/10.1029/2011GL047189.

Schumann, U., Graf, K., 2013. Aviation-induced cirrus and radiation changes at diurnal timescales. J. Geophys. Res.: Atmos. 118 (5), 2404–2421. https://doi.org/10.1002/jgrd.50184.

Bock, L., Burkhardt, U., 2016. Reassessing properties and radiative forcing of contrail cirrus using a climate model. J. Geophys. Res.: Atmos. 121 (16), 9717–9736. https://doi.org/10.1002/2016JD025112.

Righi, M., Hendricks, J., Sausen, R., 2013. The global impact of the transport sectors on atmospheric aerosol: simulations for year 2000 emissions. Atmos. Chem. Phys.

13 (19), 9939–9970. https://doi.org/10.5194/acp-13-9939-2013.
Schumann, U., Penner, J.E., Chen, Y., Zhou, C., Graf, K., 2015. Dehydration effects from contrails in a coupled contrail–climate model. Atmos. Chem. Phys. 15, 11179–11199. https://doi.org/10.5194/acp-15-11179-2015.
Appleman, H., 1953. The formation of exhaust condensation trails by jet aircraft. Bull. Amer. Meteor. Soc. 34.
Schmidt, E., 1941. Die Entstehung von Eisnebel aus den Auspuffgasen von Flugmotoren. In: Schriften der Deutschen Akademie der Luftfahrtforschung. Verlag R. Oldenbourg, Berlin, pp. 1–15.
Gierens, K.M., Lim, L., Eleftheratos, K., 2008. A review of various strategies for contrail avoidance. Open Atmos. Sci. J. 2, 1–7.
Mannstein, H., Spichtinger, P., Gierens, K., 2005. A note on how to avoid contrail cirrus. Transport. Res. Part D: Transp. Environ. 10 (5), 421–426.
Sridhar, B., Ng, H., Chen, N., 2011. Aircraft trajectory optimization and contrails avoidance in the presence of winds. J. Guidance Control Dyn. 34 (5), 1577–1584. https://doi.org/10.2514/1.53378.
Chen, N.Y., Sridhar, B., Ng, H.K., 2012. Tradeoff between contrail reduction and emissions in United States national airspace. J. Aircraft 49 (5), 1367–1375. https://doi.org/10.2514/1.C031680.
Gao, H., Hansman, R. John, 2013. Aircraft cruise phase altitude optimization considering contrail avoidance. Secondary Aircraft Cruise Phase Altitude Optimization Considering Contrail Avoidance, ICAT-2013-10. Massachusetts Institute of Technology.
Campbell, S.E., Bragg, M.B., Neogi, N.A., 2013. Fuel-optimal trajectory generation for persistent contrail mitigation. J. Guidance Control Dyn. 36 (6), 1741–1750. https://doi.org/10.2514/1.55969.
Zou, B., Buxi, G.S., Hansen, M., 2016. Optimal 4-D aircraft trajectories in a contrail-sensitive environment. Networks Spatial Econ. 16 (1), 415–446. https://doi.org/10.1007/s11067-013-9210-x.
Hartjes, S., Hendriks, T., Visser, D., 2016. Contrail mitigation through 3D aircraft trajectory optimization. 16th AIAA Aviation Technology, Integration, and Operations Conference. American Institute of Aeronautics and Astronautics, Washington, D.C., USA. http://doi.org/10.2514/6.2016-3908.
Jöckel, P., Kerkweg, A., Pozzer, A., Sander, R., Tost, H., Riede, H., Baumgaertner, A., Gromov, S., Kern, B., 2010. Development cycle 2 of the modular earth submodel system (MESSy2). Geosci. Model Dev. 3 (2), 717–752. https://doi.org/10.5194/gmd-3-717-2010.
Roeckner, E., Brokopf, R., Esch, M., Giorgetta, M., Hagemann, S., Kornblueh, L., Manzini, E., Schlese, U., Schulzweida, U., 2006. Sensitivity of simulated climate to horizontal and vertical resolution in the ECHAM5 atmosphere model. J. Clim. 19 (16), 3771–3791. https://doi.org/10.1175/JCLI3824.1.
Roeckner, E., Bäuml, G., Bonaventura, L., Brokopf, R., Esch, M., Giorgetta, M., Hagemann, S., Kirchner, I., Kornblueh, L., Manzini, E., 2003. The atmospheric general circulation model ECHAM 5. Part I: model description. Secondary The atmospheric general circulation model ECHAM 5. PART I: Model description, Report No. 349. Max Planck Institute for Meteorology, Hamburg.
Lamarque, J.-F., Dentener, F., McConnell, J., Ro, C.-U., Shaw, M., Vet, R., Bergmann, D., Cameron-Smith, P., Dalsoren, S., Doherty, R., Faluvegi, G., Ghan, S.J., Josse, B., Lee, Y.H., MacKenzie, I.A., Plummer, D., Shindell, D.T., Skeie, R.B., Stevenson, D.S., Strode, S., Zeng, G., Curran, M., Dahl-Jensen, D., Das, S., Fritzsche, D., Nolan, M., 2013. Multi-model mean nitrogen and sulfur deposition from the Atmospheric Chemistry and Climate Model Intercomparison Project (ACCMIP): evaluation of historical and projected future changes. Atmos. Chem. Phys. 13, 7997–8018. https://doi.org/10.5194/acp-13-7997-2013.
Jöckel, P., Tost, H., Pozzer, A., Kunze, M., Kirner, O., Brenninkmeijer, C.A.M., Brinkop, S., Cai, D.S., Dyroff, C., Eckstein, J., Frank, F., Garny, H., Gottschaldt, K.-D., Graf, P., Grewe, V., Kerkweg, A., Kern, B., Matthes, S., Mertens, M., Meul, S., Neumaier, M., Nützel, M., Oberländer-Hayn, S., Ruhnke, R., Runde, T., Sander, R., Scharffe, D., Zahn, A., 2016. Earth system chemistry integrated modelling (ESCiMo) with the modular Earth submodel system (MESSy) version 2.51. Geosci. Model Dev. 9 (3). https://doi.org/10.5194/gmd-9-1153-2016.
Yamashita, H., Grewe, V., Jöckel, P., Linke, F., Schaefer, M., Sasaki, D., 2016. Air traffic simulation in chemistry-climate model EMAC 2.41: AirTraf 1.0. Geosci. Model Dev. 9 (9), 3363–3392. https://doi.org/10.5194/gmd-9-3363-2016.
Grewe, V., Frömming, C., Matthes, S., Brinkop, S., Ponater, M., Dietmüller, S., Jöckel, P., Garny, H., Tsati, E., Dahlmann, K., 2014. Aircraft routing with minimal climate impact: the REACT4C climate cost function modelling approach (V1. 0). Geosci. Model Dev. 7, 175–201.
Eurocontrol, 2011. User manual for the base of aircraft data (BADA) revision 3.9. In: EEC Technical/Scientific Report.
Deidewig, F., Döpelheuer, A., Lecht, M., 1996. Methods to assess aircraft engine emissions in flight. In: 20th Congress of the International Council of the Aeronautical Sciences, Sorrento, Italy, pp. 131–141.
ICAO technical report, 2005. ICAO engine exhaust emission data. Secondary ICAO technical report-ICAO Engine Exhaust Emission Data, Doc 9646-AN/943. ICAO, Montreal, QC, Canada.
Vincenty, T., 1975. Direct and inverse solutions of geodesics on the ellipsoid with application of nested equations. Surv. Rev. 23 (176), 88–93. https://doi.org/10.1179/sre.1975.23.176.88.
Yamashita, H., Grewe, V., Jöckel, P., Linke, F., Schaefer, M., Sasaki, D., 2015. Towards climate optimized flight trajectories in a climate model: AirTraf. USA/Europe Air Traffic Management Research and Development Seminar.
Sasaki, D., Obayashi, S., Nakahashi, K., 2002. Navier-Stokes optimization of supersonic wings with four objectives using evolutionary algorithm. J. Aircraft 39 (4), 621–629.
Sasaki, D., Obayashi, S., 2005. Efficient search for trade-offs by adaptive range multi-objective genetic algorithms. J. Aerospace Comput. Inf. Commun. 2 (1), 44–64. https://doi.org/10.2514/1.12909.
Sridhar, B., Ng, H.K., Linke, F., Chen, N.Y., 2014. Benefits analysis of wind-optimal operations for trans-atlantic flights. 14th AIAA Aviation Technology, Integration, and Operations Conference. American Institute of Aeronautics and Astronautics.
Jelinek, F., Carlier, S., Smith, J., 2004. Eurocontrol experimental centre advanced emission model (AEM3) v1.5 validation report. In: Secondary Eurocontrol Experimental Centre Advanced Emission Model (AEM3) v1.5 Validation Report, EUROCONTROL, EEC Report EEC/SEE/2004/004, pp. 1–79.
Aircraft Contrails Factsheet, 2000. In: Secondary Aircraft Contrails Factsheet, Environmental Protection Agency, EPA430-F-00-005. Air and Radiation (6205J).
Frömming, C., Ponater, M., Burkhardt, U., Stenke, A., Pechtl, S., Sausen, R., 2011. Sensitivity of contrail coverage and contrail radiative forcing to selected key parameters. Atmos. Environ. 45 (7), 1483–1490. https://doi.org/10.1016/j.atmosenv.2010.11.033.
Myhre, G., Kvalevåg, M., Rädel, G., Cook, J., Shine, K.P., Clark, H., Karcher, F., Markowicz, K., Kardas, A., Wolkenberg, P., Balkanski, Y., Ponater, M., Forster, P., Rap, A., de Leon, R.R., 2009. Intercomparison of radiative forcing calculations of stratospheric water vapour and contrails. Meteorologische Zeitschrift 18 (06), 585–596. https://doi.org/10.1127/0941-2948/2009/0411.
Fichter, C., Marquart, S., Sausen, R., Lee, D.S., 2005. The impact of cruise altitude on contrails and related radiative forcing. Meteorologische Zeitschrift 14 (4), 563–572.
Danielsen, E.F., 1968. Stratospheric-tropospheric exchange based on radioactivity, ozone and potential vorticity. J. Atmos. Sci. 25 (3), 502–518. https://doi.org/10.1175/1520-0469(1968) 025<0502:STEBOR>2.0.CO;2.
škerlak, B., Sprenger, M., Pfahl, S., Tyrlis, E., Wernli, H., 2015. Tropopause folds in ERA-Interim: global climatology and relation to extreme weather events. J. Geophys. Res.: Atmos. 120 (10), 4860–4877. https://doi.org/10.1002/2014JD022787.
Sridhar, B., Chen, N.Y., Ng, H.K., 2011. Energy efficient strategies for reducing the environmental impact of aviation. In: 10th USA/Europe Air Traffic Management Research and Development Seminar, Chicago, IL, USA, pp. 1–10.
Sridhar, B., Chen, N.Y., 2010. Fuel efficient strategies for reducing contrail formations in United States airspace. 29th Digital Avionics Systems Conference, Salt Lake City, UT, USA. . http://doi.org/10.1109/DASC.2010.5655533.
Dahlmann, K., Grewe, V., Frömming, C., Burkhardt, U., 2016. Can we reliably assess climate mitigation options for air traffic scenarios despite large uncertainties in atmospheric processes? Transport. Res. Part D: Transp. Environ. 46 (Suppl. C), 40–55. https://doi.org/10.1016/j.trd.2016.03.006.
Grewe, V., Matthes, S., Frömming, C., Brinkop, S., Jöckel, P., Gierens, K., Champougny, T., Fuglestvedt, J., Haslerud, A., Irvine, E., Shine, K., 2017. Feasibility of climate-optimized air traffic routing for trans-Atlantic flights. Environ. Res. Lett. 12 (3).
Frömming, C., Ponater, M., Dahlmann, K., Grewe, V., Lee, D.S., Sausen, R., 2012. Aviation-induced radiative forcing and surface temperature change in dependency of the emission altitude. J. Geophys. Res.: Atmos. 117 (D19), 1–15. https://doi.org/10.1029/2012JD018204.
Schumann, U., Graf, K., Mannstein, H., 2011. Potential to reduce the climate impact of aviation by flight level changes. 3rd AIAA Atmospheric Space Environments

Conference. American Institute of Aeronautics and Astronautics, Honolulu, Hawaii. http://doi.org/10.2514/6.2011-3376.
Lührs, B., Niklass, M., Froemming, C., Grewe, V., Gollnick, V., 2016. Cost-benefit assessment of 2D and 3D climate and weather optimized trajectories. 16th AIAA Aviation Technology, Integration, and Operations Conference. American Institute of Aeronautics and Astronautics, Washington, D.C., USA. http://doi.org/10.2514/6.2016-3758.
Meerkötter, R., Schumann, U., Doelling, D.R., Minnis, P., Nakajima, T., Tsushima, Y., 1999. Radiative forcing by contrails. Annales Geophysicae 17 (8), 1080–1094. https://doi.org/10.1007/s00585-999-1080-7.
Rap, A., Forster, P.M., Jones, A., Boucher, O., Haywood, J.M., Bellouin, N., De Leon, R.R., 2010. Parameterization of contrails in the UK Met Office Climate Model. J. Geophys. Res.: Atmos. 115 (D10). https://doi.org/10.1029/2009JD012443.
Myhre, G., Stordal, F., 2001. On the tradeoff of the solar and thermal infrared radiative impact of contrails. Geophys. Res. Lett. 28 (16), 3119–3122. https://doi.org/10.1029/2001GL013193.
Stuber, N., Forster, P., Rädel, G., Shine, K., 2006. The importance of the diurnal and annual cycle of air traffic for contrail radiative forcing. Nature 441 (7095), 864–867.
Grewe, V., Champougny, T., Matthes, S., Frömming, C., Brinkop, S., Søvde, O.A., Irvine, E.A., Halscheidt, L., 2014. Reduction of the air traffic's contribution to climate change: a REACT4C case study. Atmos. Environ. 94, 616–625. https://doi.org/10.1016/j.atmosenv.2014.05.059.
Haywood, J.M., Allan, R.P., Bornemann, J., Forster, P.M., Francis, P.N., Milton, S., Rädel, G., Rap, A., Shine, K.P., Thorpe, R., 2009. A case study of the radiative forcing of persistent contrails evolving into contrail-induced cirrus. J. Geophys. Res.: Atmos. 114 (D24). https://doi.org/10.1029/2009JD012650.
Köhler, M.O., Rädel, G., Dessens, O., Shine, K.P., Rogers, H.L., Wild, O., Pyle, J.A., 2008. Impact of perturbations to nitrogen oxide emissions from global aviation. J. Geophys. Res.: Atmos. 113 (D11), 1–15. https://doi.org/10.1029/2007JD009140.